ELSEVIER

Cement and Concrete Composites **19** (1997) 69–79

0958-9465/97/$17.00+0.00

PII:S0958-9465(96)00043-1

Implementation of EFPI-based Optical-fiber Sensor Instrumentation for the NDE of Concrete Structures

Marten de Vries,[a] Vivek Arya,[a] Scott Meller,[a] Sami F. Masri[b] & Richard O. Claus[a]

[a]Fiber and Electro-Optics Research Center, Bradley Department of Engineering, Virginia Polytechnic Institute and State University, Blacksburg, VA 24061-0356, USA
[b]Department of Civil Engineering, University of Southern California, Los Angeles, CA 90089, USA

Abstract

This paper reports on the design and implementation of an optical-fiber sensor based on the extrinsic Fabry–Perot interferometer (EFPI) for the non-destructive quantitative evaluation of advanced concrete-based civil structures. The performance of the EFPI sensor is demonstrated in two different applications. In the first implementation, performed with researchers in the Civil Engineering Department at the University of Southern California in Los Angeles, optical-fiber sensors were used to obtain quantitative strain information from reinforced concrete interior and exterior column-to-beam connections. The second implementation, performed in co-operation with researchers at the Turner Fairbanks Federal Highway Administration Center in McLean, Virginia, used optical-fiber sensors, attached to composite prestressing strands used for reinforcing concrete, to obtain absolute strain information. The paper is concluded with a discussion of practical considerations that need to be taken into account when implementing optical-fiber sensors in a concrete civil structure environment. © *1997 Published by Elsevier Science Limited*

Keywords: optical fiber sensors, non-destructive evaluation, smart materials and structures, strain monitoring.

INTRODUCTION

Optical-fiber sensors, unlike conventional electrically-based sensors, are fabricated with high-strength silica which possesses an inherent immunity to corrosion and electromagnetic interference. Their small size and geometric flexibility allows them to be embedded unobtrusively in or attached to the surface of the host structure. Fiber-optic sensors have been used for the non-destructive evaluation (NDE) of advanced materials and structures for over 10 years.[1] For example, in composites, fiber sensors have been demonstrated to be feasible for the measurement of internal material changes during fabrication, the in-service lifetime measurement of strain, temperature, vibration, and other physical perturbations, and the eventual detection of damage or property degradation.[2] Recent advances in fiber-optics communication technology and the widespread use of fiber communications have made available a large selection of reliable and inexpensive opto-electronic devices and components for use in sensors and sensor instrumentation support systems.

Composite materials have found extensive applications in the high-technology defense industry. Especially in the military aerospace industry, where cost is less important than performance, composite materials have been implemented because of their light weight, high specific strength, excellent fatigue behavior, low thermal expansion, and good resistance to corrosion and a variety of chemicals.[3] Advanced composite materials are also quickly replacing traditional materials in the commercial sporting goods market, where the cost vs performance factor is much more important. So far, though,

owing to liability concerns, higher up-front costs, unfamiliar design procedures, and a lack of long-term reliability data, few civil structures have been designed with composite materials. Plans to build these types of structures, however, are underway. For example in San Diego, California, a cable-stayed, 60 ft wide, 450 ft long all-composite bridge is being designed, and will be built, to connect the two campuses of the University of California at San Diego across route I-5.[4] Composites are ideal for larger structural facilities where weight considerations are an issue. But composite materials are also used to retrofit and augment existing structures and in some cases are making the structures stronger than before.

Since limited information is available on composite materials and few models can accurately predict their durability, it is important to implement monitoring systems that can non-destructively determine the structural integrity of such advanced materials. It has already been shown that optical-fiber sensors are ideal candidates for embedding in composite materials to monitor structural health.[5] In the case of advanced civil structures that implement all-composite designs optical-fiber sensors would be ideal for monitoring structural integrity since few models can accurately determine the integrity of the structure over time.

A growing number of researchers are now embedding optical-fiber sensors into concrete civil structures to monitor various physical perturbations in the structures.[6,7] Even though most of this work is qualitative in nature, results show great promise. Relatively low-cost fiber-optic refractive index sensors have been developed by Ansari *et al.* at the New Jersey Institute of Technology in Newark, for the *in situ* determination of air content in fresh concrete.[8] Researchers have implemented polarimetric-type optical-fiber sensors that can be used to monitor stress concentrations in small concrete specimens. The orientation of the birefringent axis is extremely important and difficult to align, making this type of sensor difficult to implement in large structures outside the laboratory.[9,10]

Sensors embedded in concrete that are not attached to rebar, or some other type of reinforcing material, may not provide accurate, reliable or long-term information related to the parameters they are trying to monitor. Mendez and Morse, and Huston *et al.* have both already indicated that, for accurate and reliable measurements, it is essential to ensure that there is adequate and stable strain/state transfer between the host structure and the fiber-sensor elements.[11,12] In fact, Majumdar reports that in concrete the interfacial bond between the glass fiber and matrix material is poor since the bond is both discontinuous and irregular.[13] If the interfacial bond between the fiber and the concrete was good, cracks that typically occur in concrete over time, and that are expected, would propagate through the fiber and destroy the sensor.

Despite these problems, however, progress in embedding optical-fiber sensors in concrete has been made. Fuhr *et al.*, at the University of Vermont, were able to detect vibration signatures from turbine engines used in a dam using modal-domain-based optical-fiber sensors embedded in the dam wall.[14] Measures *et al.*,[15] using Bragg-type gratings, and Wolff and Miesseler,[16] using optical time-domain reflectometry techniques, were able to perform strain measurements on composite prestressing strands used to reinforce concrete bridges. Even though both techniques can be used to obtain strain information, both systems require complex temperature compensation techniques to obtain truly quantitative strain information.

This paper discusses the use of optical-fiber sensors for the non-destructive quantitative evaluation of advanced civil structures. It covers a wide range of issues pertaining to sensors embedded in, and attached to, these structures.

EXTRINSIC FABRY–PEROT INTERFEROMETER

Optical-fiber-based Fabry–Perot sensors reported in the literature have been shown to be highly sensitive to temperature, strain, vibration, acoustic waves and magnetic fields.[17] The fabrication of these Fabry–Perot-type sensors has typically been achieved with the use of air–glass reflectors,[18] in-fiber Bragg gratings,[19] or through the use of semi-reflective splices along the length of the fiber.[20] In extrinsic sensors, the fiber only serves to carry optical power to, and sensing information from, an external region, usually air. The main advantages of the extrinsic method over the intrinsic method include the avoidance of polarization problems, and the detection of the axial strain components

only. For the extrinsic Fabry–Perot interferometer (EFPI), first described by Murphy, the Fabry–Perot cavity is formed between the air–glass interfaces of two fiber endfaces aligned in a hollow-core fiber.[21] Changes in the separation between the two fiber endfaces, known as the gap length, cause interferometric fringe variations. In this section we present a theoretical analysis of the optical field reflected off the target fiber using Kirchhoff's diffraction theory. This analysis allows the prediction of the signal-to-noise ratio as a function of the gap length and helps in determining the dynamic range of a given sensor. Experimental results which support the theoretical predictions are also presented.

The EFPI sensor geometry is shown in Fig. 1. Here light from a 1300 nm laser light source is coupled into the sensor head which consists of a 126 μm inner diameter hollow-core tube into which a 9/125 μm single-mode input fiber and a second fiber, serving solely as a reflector, are positioned. The reflection, approximately 4%, from the first glass–air interface at the end of the input fiber, R_1, and the reflection, R_2, from the air–glass interface at the input to the second fiber interfere and couple back to a detector via a 2×2 coupler. The resulting interference signal varies sinusoidally in response to microdisplacements in the air-gap cavity. Typical interference fringes observed for displacing the sensor from 0 to 400 μm are shown in Fig. 3. In these experiments the target fiber was not bonded to the hollow-core fiber so that it could slide freely inside the hollow-core fiber.

EFPI sensor analysis

The theoretical analysis of EFPI-based optical-fiber sensors has conventionally been performed by the vectorial summation of the two reflected fields, R_1 and R_2. This is, however, a simplified

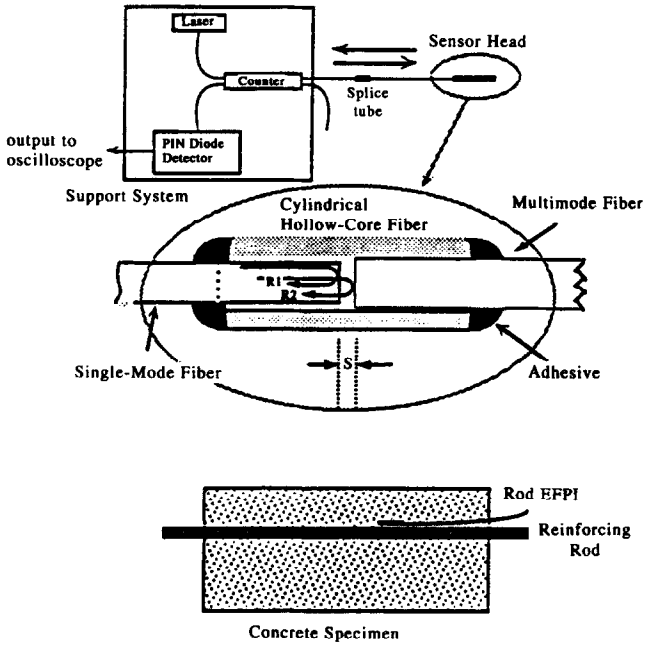

Fig. 1. Extrinsic Fabry–Perot interferometric sensor geometry.

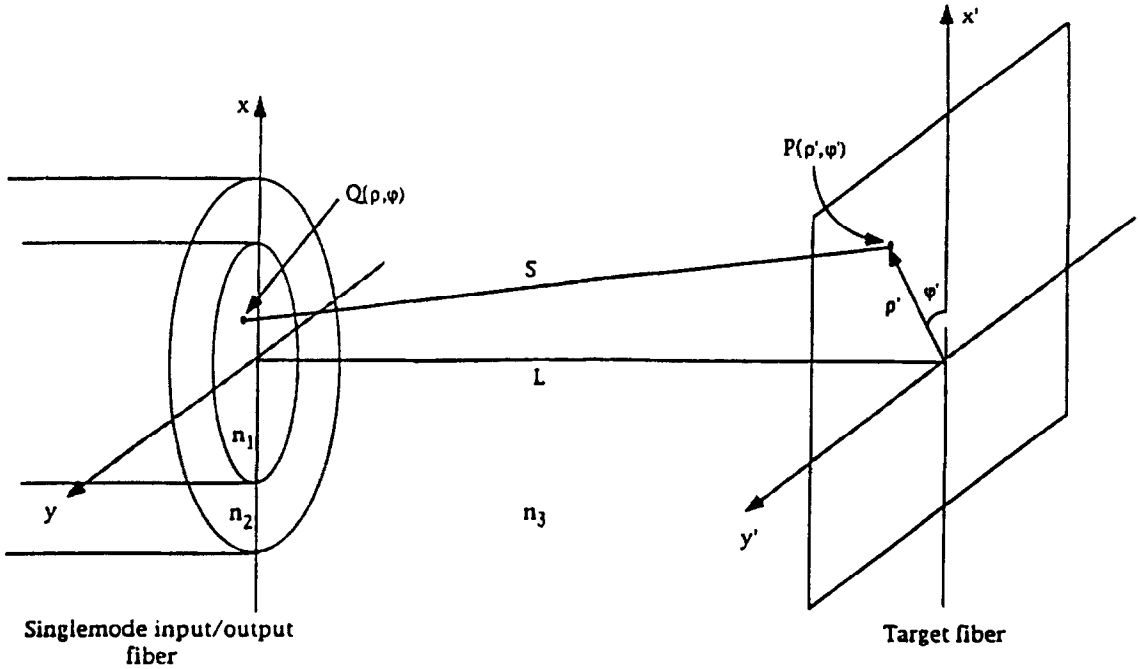

Fig. 2. Coordinate system for the Kirchhoff analysis.

model since it approximates the reflections in the Fabry–Perot (FP) cavity with only a two-beam model, and hence an exact analysis was performed using an approach based on Kirchhoff's diffraction formalism.[22] As shown in this section, the exact approach yields results which are in closer agreement with those obtained experimentally, compared with the conventional two-beam interference approach.

For a weakly-guiding, circular-core optical fiber, the scalar field of the fundamental mode, LP_{01}, can be assumed to be approximately Gaussian in shape, given by[23]

$$\Psi_{01} = A \exp\left(\frac{-\rho^2}{\omega^2}\right) \exp(-j\beta z). \qquad (1)$$

where ω is the mode field radius, A is the normalized amplitude, β is the modal propagation constant, ρ and z are cylindrical coordinates, and the temporal dependence is implicit. Assuming that the electric field at the endface of the input (lead-in) fiber can be expressed by eqn (1), the electric field at any point P outside the lead-in fiber endface is given by Kirchhoff's diffraction formula[24]

$$\Psi(P) = \frac{1}{4\pi} = \int\int \left[\Psi_{01} \frac{\partial}{\partial z}\left(\frac{\exp(jkS)}{S}\right) - \frac{\exp(jkS)}{\partial z} \frac{\partial \Psi_{01}}{\partial z}\right] \mathrm{d}s. \qquad (2)$$

In the above equation, $k = 2\pi/\lambda$ is the free space propagation constant, and the integral is evaluated over the lead-in fiber endface region. Using eqn (1), eqn (2) may be simplified to be of the form

$$\Psi(P) = \int\int \left[\Psi_{01}\left(\frac{\exp(jkS)}{S}\right) \left\{\frac{2L}{S}\left(jk - \frac{1}{S}\right) + jk\right\}\right] \mathrm{d}s, \qquad (3)$$

where L is the gap length of the Fabry–Perot cavity. The factor S is the vector distance between a point Q at the input/output endface and the point P, as shown in Fig. 2. From geometry, S can be written as

$$S = \sqrt{\rho^2 + (\rho')^2 - 2\rho\rho' \cos(\phi - \phi') + (z - z')^2}, \qquad (4)$$

where ρ, ϕ, and z are the cylindrical coordinates at the lead-in fiber endface, and ρ', ϕ', and z' are the cylindrical coordinates at the point P. Use of the Gaussian approximation for the guided fundamental mode field ensures that light propagating in the cladding is also accounted for while evaluating the integrals. The target fiber in Fig. 2 acts as a partial reflector with a Fresnel reflection of approximately 4%. The normalized electric field amplitude, A', at this reflector may be expressed as

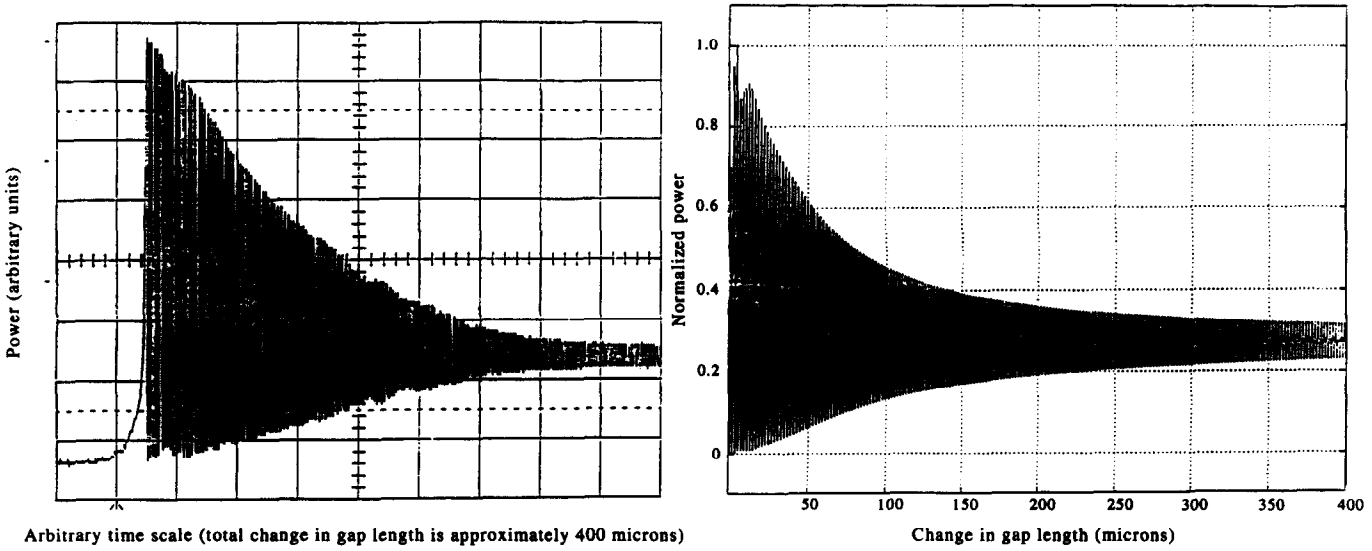

Fig. 3. Experimental (left) and theoretical (right) results of output power vs gap length (0–400 μm).

$$A' = \frac{\int\int \left[\Psi(P)\exp\left(-\left(\frac{\rho'^2}{\omega^2}\right)\right)\right] ds'}{\int\int \left[\exp\left(-\left(\frac{\rho'^2}{\omega^2}\right)\right)\right]^2 ds'}. \quad (5)$$

The total field at the input/output fiber may then be expressed as the summation of E_i, the field due to the first reflection at the glass/air interface, and E_r, the field contributed by the target fiber at this interface. These fields may be written as

$$E_i = C\Psi_{01}, \quad (6)$$

and

$$E_r = C(1-C^2)|A'|\Psi_{01}\exp(jk_0L), \quad (7)$$

where $C = (n_f - n_o)/(n_f + n_o)$ is the Fresnel reflection coefficient at the air/glass interface of the fiber. For a typical silica fiber, C is approximately 0.2. Hence using eqns (6) and (7), the total optical power returning through the input/output fiber is given by

$$P_{total} = \iint I\, ds = \iint |E_i + E_r|^2\, ds, \quad (8)$$

where I represents the intensity contributed by the two reflections at a given point on the endface of the fiber mode field, and the integral is calculated over the endface of this mode field. The gap length, L, is half the axial distance used for the Kirchhoff integral [eqn (2)]. A program was written to perform the numerical calculation of eqn (8). The resulting normalized power vs gap length for displacements from 0 to 400 μm are shown in Fig. 3. The theoretical graph shown in Fig. 3 shows oscillations in the near field which indicate the presence of Fresnel zones.[25] The reason for their absence in the experiment could be axial misalignment between the input/output and target fiber due to imperfect fiber endface cleaves and hollow-core tube attachment. This observation is important since, for given fiber parameters, the numerical analysis yields the minimum gap length for reliable sensor operation. The experimental fringe contrast vs gap length, along with the theoretical prediction, is illustrated in Fig. 4. The experimental fringe contrast decreases

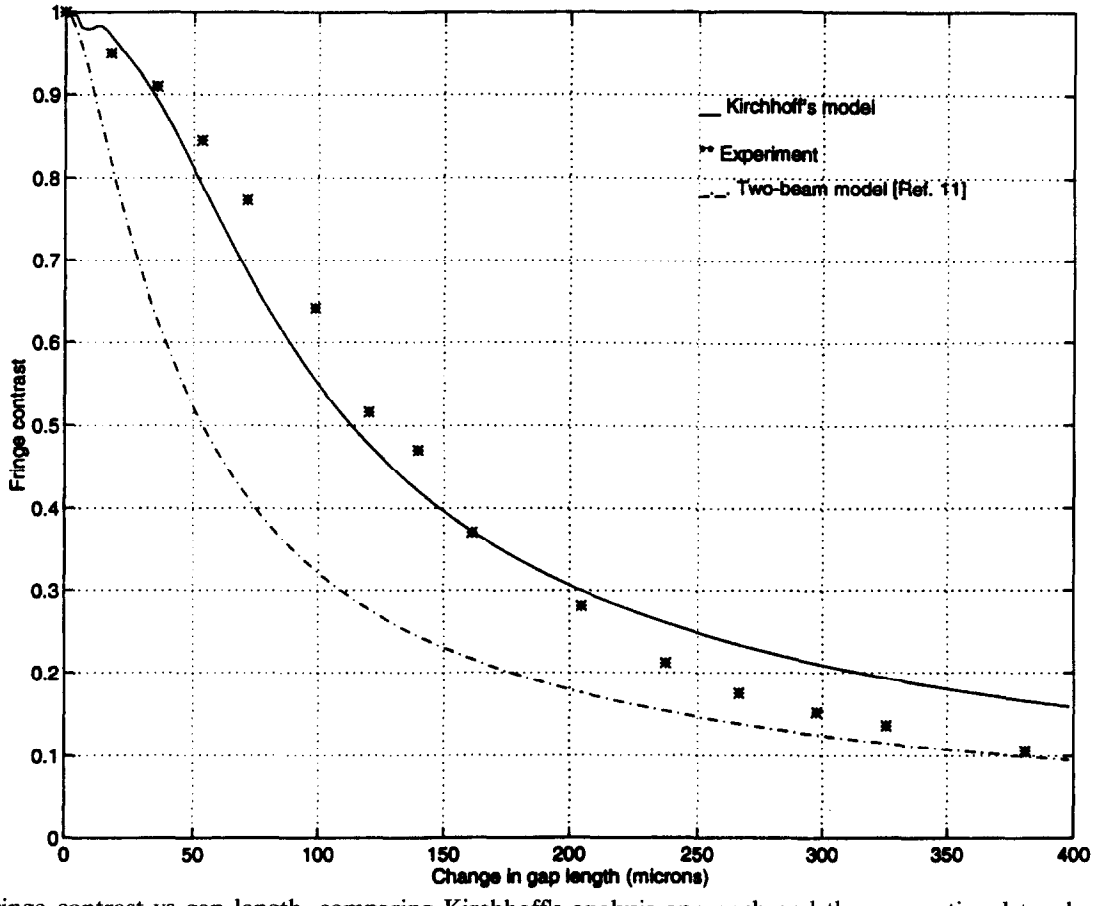

Fig. 4. Fringe contrast vs gap length, comparing Kirchhoff's analysis approach and the conventional two-beam analysis with experimental results.

more rapidly as compared with the theory. This could be due to increasing misalignment between the input/output and target fibers.

EFPI sensor implementation

A full-scale external-reinforced concrete column–beam interconnect specimen, shown in Fig. 5, was designed and constructed at the USC Civil Engineering Department in Los Angeles. A rebar cage was constructed and EFPI strain gages, with collocated foil strain gages, were placed on the main rebar, and selected beam and column stirrups. The rebar and stirrup surfaces were ground to the required smoothness at the appropriate gage positions, prior to attachment, and a silicone rubber layer was used for waterproofing the sensors. Figure 6 shows the locations of the fiber-optic strain gages. As a result of unforeseen delays, the specimen was not poured with concrete for six months after the sensors had been attached, and the actual tests were not performed until three months after the concrete had set. These delays did not affect the performance of the gages.

The EFPI strain gages were configured to yield only the strain component parallel to the long axis of the rod on which it was attached. To determine which sensors had survived the embedding process, small cyclic loads were applied to the specimen. All sensors showed a response. With the set-up used only two sensors could be monitored, and it was therefore decided to dedicate one channel to monitoring one sensor throughout the entire test and to use the other channel to periodically switch over to the other sensors.

Specimen dimensions, as given in Fig. 6, were 8 in × 16 in × 63 in for the beam, and 12 in × 12 in × 108 in for the column. The column-to-beam interconnection was tested in the vertical plane. The beam tip was displaced at a constant rate and a periodic loading cycle was used for the beam-tip displacements.

Typical comparative strain data obtained from sensor 6 and sensor 4 for beam tip displacement from 0 to 0.5 in are shown in Fig. 7. Here, note the general agreement between sensor 6 (upper graph) and sensor 4 (lower graph). The upper traces on both graphs are expansions of the lower traces. The lead-out fiber for sensor 4 was destroyed during the −2 to 2 in loading cycle series. Figure 8 summarizes all the data obtained from fiber-optic sensor 6. The horizontal axis indicates the maximum displacement of the beam, as it was displaced from its minimum position, through zero, to its maximum position. The vertical axis accounts for the total change in strain as the beam moves from its minimum to its maximum position and consists of both compressive and tensile strain.

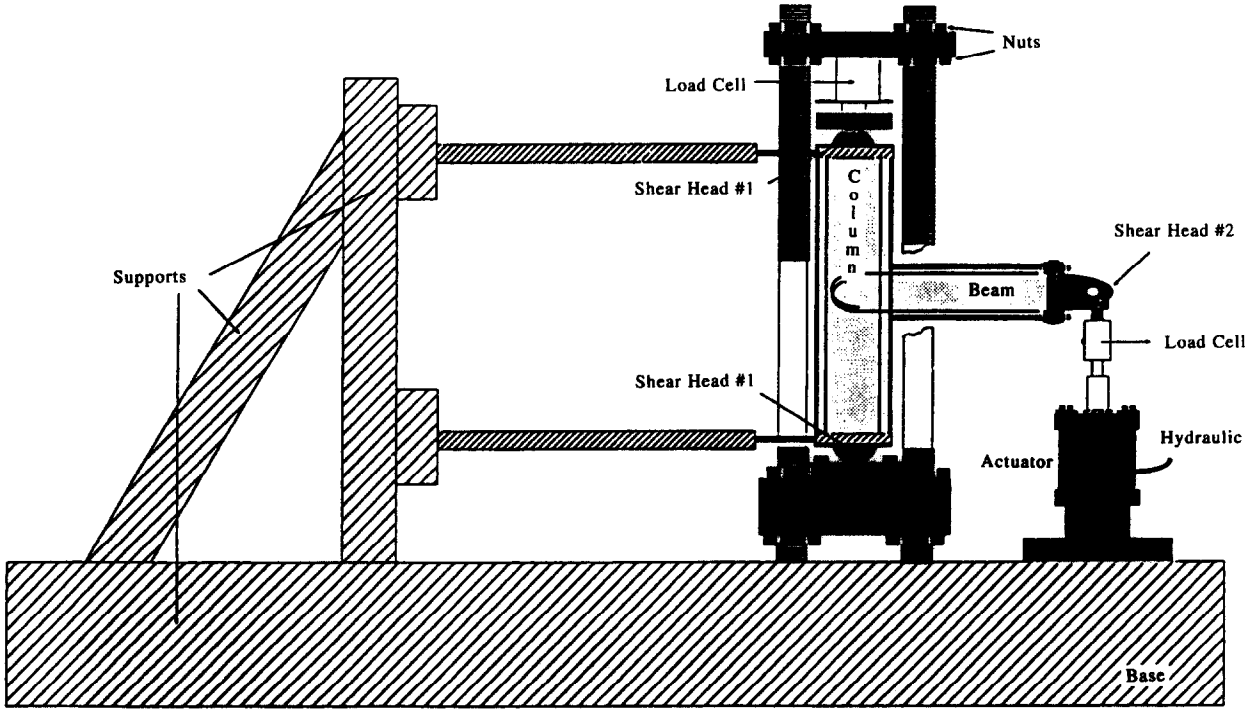

Fig. 5. Overview of the external column-to-beam set-up used to impose dynamic loads.

Unfortunately, for this experiment, data from the foil strain gages were not available for comparison. The foil strain gage did survive the specimen fabrication process, but, possibly due to improper installation procedures, none of the gages was able to provide reliable data.

ABSOLUTE EXTRINSIC FABRY–PEROT INTERFEROMETER

The standard EFPI implemented in the previous experiment is unable to provide absolute measurements and may be susceptible to directional ambiguity. Moreover, when the system is turned off, all the phase information is lost and hence it is impossible to obtain absolute strain data for long-term field-test measurements. These drawbacks have focused current research in optical-fiber sensors on absolute optical-fiber sensors which yield non-relative strain information.

Absolute EFPI sensor analysis

The following provides a brief analysis of the absolute EFPI (AEFPI) system used in this experiment. An in-depth analysis of the AEFPI sensor is given by Bhatia *et al.*[26] The intensity, I, at the output of an EFPI is described by

$$I = I_0 \cos\left(\frac{4\pi}{\lambda} L\right), \tag{9}$$

where I_0 is the maximum value of the output intensity, L is the gap separation, and λ is the laser-diode center wavelength. A change in the

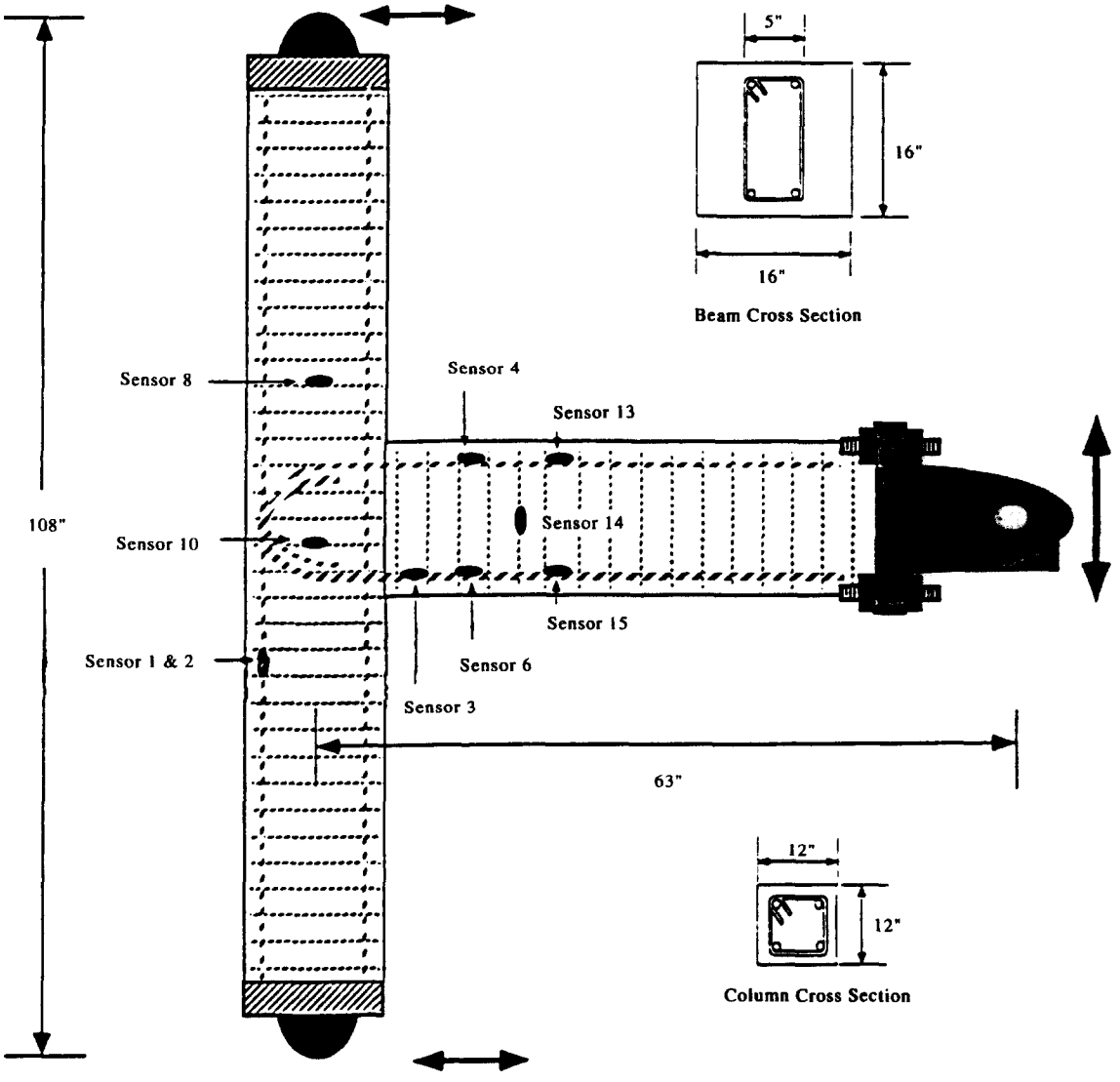

Fig. 6. Dimensions of the specimen and location of the fiber-optic and collocated foil strain gage sensors.

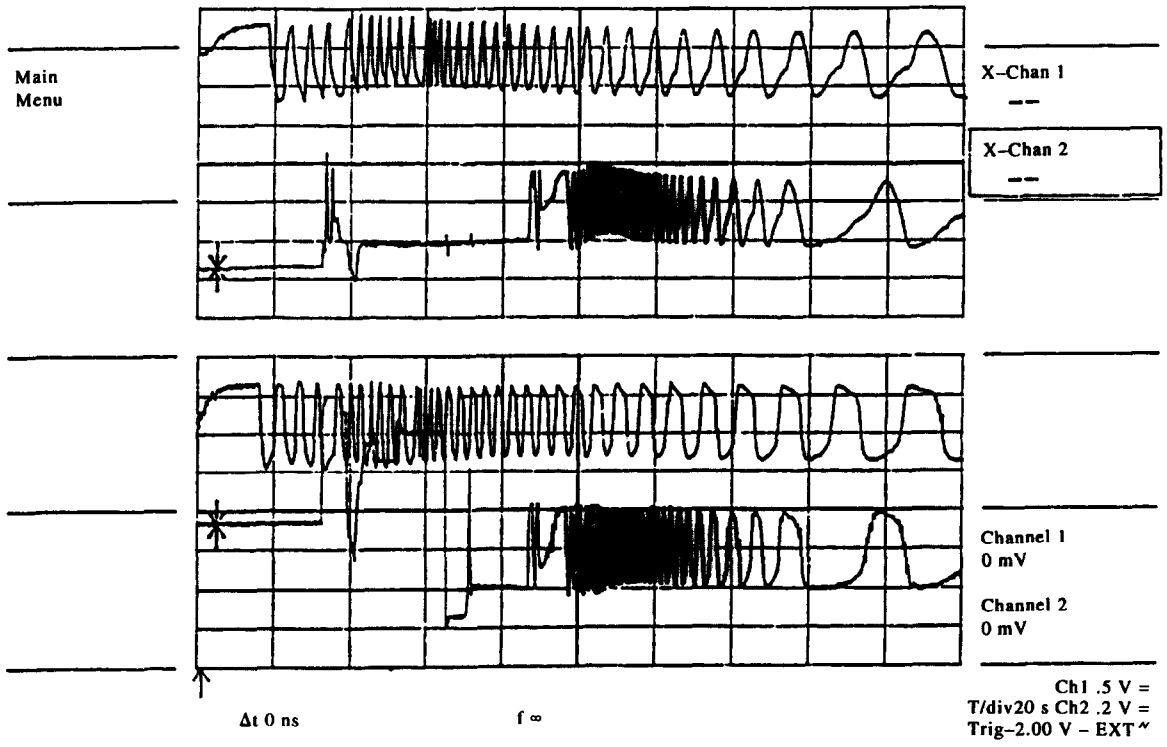

Fig. 7. Comparative strain data obtained from sensor 6 (top graph) and sensor 4 (bottom graph), for beam-tip displacement from 0 to 0.5 in.

gap separation, L, caused by an external perturbation such as strain, results in a sinusoidal modulation of the output intensity, I. If a change in direction of the applied strain occurs at a maximum or a minimum the system will be unable to detect it. Still, the EFPI system can only be used to monitor relative strain changes, and cannot be used to monitor absolute strain; once the EFPI system is turned off, strain information is lost. The AEFPI system uses a superluminscent diode (SLED) instead of a laser diode and is based on the concept of white light interferometry. The signal processing is done using a spectrometer, followed by a personal computer, as shown in Fig. 9. Two wavelengths, λ_1 and λ_2, which are 2π out of phase, are determined from the spectrometer and the gap separation, L, is calculated using

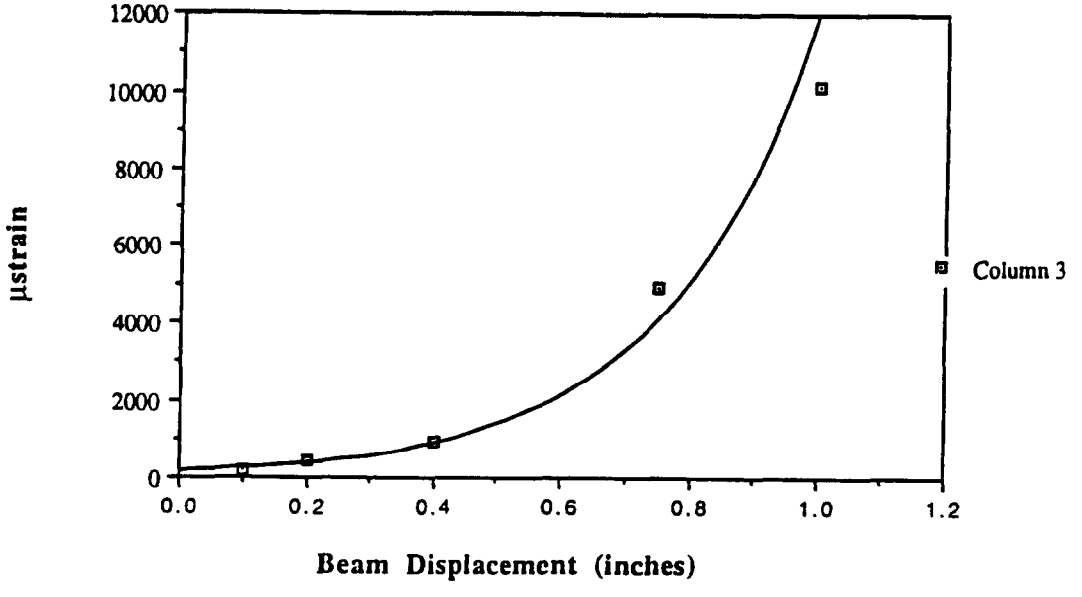

Fig. 8. Strain data from sensor 6.

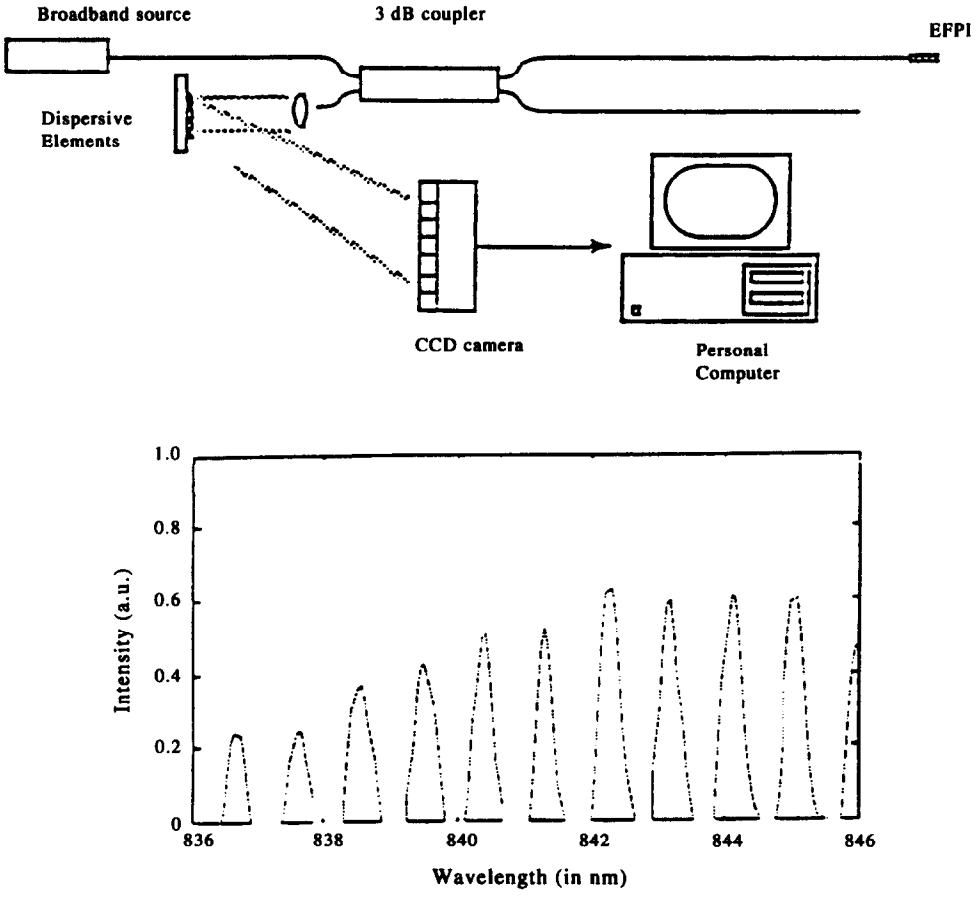

Fig. 9. Set-up of the absolute EFPI (AEFPI) system, and typical output of the AEFPI system.

$$L = \frac{(\lambda_1 \lambda_2)}{2(\lambda_2 - \lambda_1)}. \tag{10}$$

The gap separation is then used to calculate the applied strain, given the gage length of the sensor. By coating the fiber endfaces inside the hollow-core fiber with a high-purity gold, a high-finesse Fabry–Perot cavity is made. The sensitivity of the overall system can be improved by increasing the finesse, F,

$$F = \frac{\pi\sqrt{r}}{1-r}, \tag{11}$$

where r is the reflectivity of the endface.[24] Typical output response from an AEFPI sensor is shown in Fig. 9. The AEFPI system can detect temperature changes as small as 2°C and strain changes as small as 100 $\mu\epsilon$.[27] Since the system is not differential in nature, it does not require a reference measurement to be made prior to the actual sensing procedure, an absolute measurement is made each time the system is turned on. Due to the scanning time needed by the spectrum analyzer, this system is only suitable for quasi-static measurements. In the experiment described in the next section the absolute EFPI (AEFPI) was implemented.

AEFPI sensor implementation

Concrete, though strong in compression, is quite weak in tension, and compressive stress on it can be used to counterbalance any tensile force due to loading, which might lead to either cracks or deflection. Although prestressed concrete is more expensive to manufacture than reinforced concrete, the long-term savings owing to reduced maintenance and extended lifetime are making it a popular choice for use in long-span structures, such as segmented bridges.[28] In pre-tensioning prestressed concrete, a tendon is tensioned before concrete is placed and the prestress is transferred to the concrete after it has cured, usually for 8 to 10 days, by releasing the tendon. If this prestressing force is applied along the axis of the structure, the procedure is termed linear prestressing. In linear prestressing it is often

required to determine the axial strain on the tendon during the initial procedure of pre-tensioning, so that the required longitudinal force to achieve maximum concrete strength can be determined accurately.

The experiment was performed at the Turner Fairbanks Federal Highway Administration research facility located in McLean, Virginia.[29] The reinforcing of concrete was implemented using a pretensioned graphite composite strand. In order to enable survivability of the sensors in high-strain environments, the input fiber was bonded to the hollow-core fiber while the output/reflective fiber was allowed to move freely inside the hollow-core fiber by bonding it to the prestressing strand. The gage length, L, was determined by measuring the distance between the point where the input fiber was epoxied to the hollow-core fiber and the point where the output fiber was epoxied to the prestressing strand. Since the strain was not directly transferred to the glass fiber, strains in excess of 10000 $\mu\epsilon$ could be monitored. The fiber sensors were attached so that the axis of the strand and that of the hollow-core fiber were parallel to each other. Five foil strain gages were also attached at different locations on the graphite prestressing tendon.

One end of the prestressing tendon was kept anchored while the other end was loaded, so that the strand was axially strained with increasing load. The load was increased in steps of approximately 2000 lbs. The frequency of the output fringes increases with increase in load, owing to the increase in the gap length, d, and a consequent reduction in $\lambda_2 - \lambda_1$. The measured strain is plotted against the applied load in Fig. 10. The final value of strain measured by the AEFPI system was 12255 $\mu\epsilon$, which was within 2% of the value measured by a collocated foil strain gage. The strain from the AEFPI sensor was obtained in real time. It is interesting to note that two of the foil strain gages failed at higher loads.

CONCLUSION

In this paper we have demonstrated the performance of EFPI sensors in two different implementations. The results obtained from these experiments look promising but several issues still need to be taken into consideration. An optical-fiber sensor embedded in or attached to a civil structure should be able to sense condition changes reliably and accurately over the entire lifetime of the structure. The civil infrastructure environment, especially when concrete is used, is an exceptionally harsh environment. Specialty coatings are required to

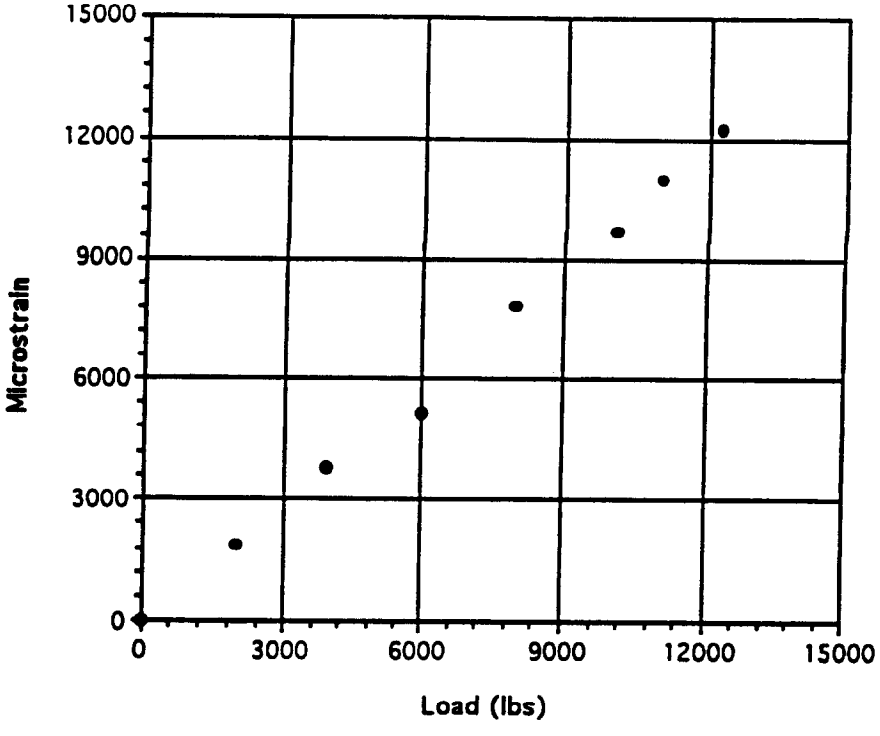

Fig. 10. Measured strain vs applied load.

protect the optical-fiber sensors from corrosion caused by the high alkaline content of the concrete. During construction, extra precautions need to be taken to ensure that the sensor itself and the lead-in/out fibers are sufficiently protected from workers, machines, weather and falling material. After construction, special care must be taken not to sever the fibers at the points where they enter or exit the structural material. Fiber fracture at these points may be the single most important problem that needs to be overcome before fiber sensors can be used for the non-destructive evaluation of structures.

REFERENCES

1. Dakin, J. & Culshaw, B., *Optical Fiber Sensors: Principles and Components*. Artech House, Boston, MA, 1988.
2. Claus, R. O., *Fiber Optic Sensor-Based Smart Materials and Structures*. IOP Publishing, Bristol and Philadelphia, April 1992.
3. Kim, P. & Meier, U., CFRP cables for large structures. In *Proc. of Advanced Composite Materials in Civil Engineering Structures*, Las Vegas, 1991, pp. 233–244.
4. Brown, A. S., Sneaking up on nondefense applications. *Aerospace America*, (March 1994) 32–42.
5. Singh, H. & Sirkis, J. S., Micromechanics of laminated composites with embedded optical fibers. In *Proc. of Smart Materials and Structures Workshop*, Blacksburg, VA, April 1991.
6. Escobar, P., Gusmeroli, V. & Martinelli, M., Fiber-optic interferometric sensors for concrete structures. In *Proc. 1st European Conf. on Smart Structures and Materials*, Glasgow, 1992, pp. 215–218.
7. Huston, D. R., Fuhr, P. L., Kajenski, P. J., Ambrose, T. P. & Spillman, W. B., Installation and preliminary results from fiber optic sensors embedded in a concrete building. In *Proc. 1st European Conf. on Smart Structures and Materials*, Glasgow, 1992, pp. 409–412.
8. Ansari, F., Rapid in-place air content determination in fresh concrete. *ACI CI*, **13**(1) (1991) 39–43.
9. Nanni, A., Yang, C. C., Pan, K., Wang, J. S. & Michael, R. R., Fiber-optic sensors for concrete strain/stress measurement. *ACI Mater. J.*, **88** (1991) 257.
10. Sirkis, J., Phase–strain–temperature model for structurally embedded interferometric optical fiber strain sensors with applications. In *Fiber Optic Smart Structures and Skins IV*, SPIE Proc. Vol. 1588, 1991, pp. 26–43.
11. Mendez, A. & Morse, T. F., Overview of optical fiber sensors embedded in concrete. In *Fiber Optic Smart Structures and Skins V*, SPIE Proc. Vol. 1798, No. 22, 1992, pp. 205–216.
12. Huston, D., Fuhr, P., Kajenski, P. & Snyder, D., Concrete beam testing with optical fiber sensors. In *Proc. Nondestructive Testing of Concrete Elements and Structures*, ASCE, San Antonio, TX, April 1992, pp. 60–69.
13. Majumdar, A. J., Glass fibre reinforced cement and gypsum products. *Proc. Roy. Soc. Lond. A*, **319** (1970) 69–78.
14. Fuhr, P. L., Huston, D. R., Ambrose, T. P. & Barker, D. A., Embedded sensors results from the Winooski One Hydroelectric Dam. In SPIE Proc. Vol. 2191, 1994, pp. 446–456.
15. Alavie, A. T., Maaskant, R., Ohn, M. M., Rizkalla, S. & Measures, R. M., Application and characterization of intracore grating sensors in a CFRP prestressed concrete girder. In SPIE Proc. Vol. 2191, 1994, pp. 103–110.
16. Wolff, R. & Miesseler, H. J., Monitoring of prestressed concrete structures with optical fiber sensors. In *Proc. 1st European Conf. on Smart Structures and Materials*, Glasgow, 1992, pp. 23–30.
17. Yoshino, T., Kurosawa, K., Itoh, K. & Ose, T., Fiber-optic Fabry–Perot interferometer and its sensor applications. *IEEE J. Quantum Electron.*, **18** (1982) 1624–1632.
18. Kersey, A. D., Jackson, D. A. & Corke, M., A simple fibre Fabry–Perot sensor. *Opt. Commun.*, **45** (1983) 71–74.
19. Belsey, K. L., Carroll, J. B., Hess, L. A., Huber, D. R. & Schmadel, D., Optically multiplexed interferometric fiber optic sensor system. *SPIE Proc.*, **566** (1985) 257.
20. Lee, C. E., Gibler, W. N., Atknis, R. A. & Taylor, H. F., In-line fiber Fabry–Perot interferometer with high reflectance internal mirrors. *J. Lightwave Technol.*, **4** (1986) 382–385.
21. Murphy, K. A., Novel phase-modulated optical fiber sensors. Ph.D. Dissertation, Virginia Polytechnic Institute and State University, Blacksburg, VA, August 1992.
22. Arya, V. & de Vries, M. *et al.*, Exact analysis of the extrinsic Fabry–Perot interferometric optical fiber sensor using Kirchhoff's diffraction formalism. *J. Opt. Fiber Technol.*, **1**(4) (1995) 380–384.
23. Marcuse, M., *Appl. Opt.*, **23** (1984) 1082–1091.
24. Born, M. & Wolf, E., *Principles of Optics*. Pergamon Press, New York, 1985.
25. Banerjee, P. P. & Poon, T. C., *Principles of Applied Optics*. Aksen Associates Inc. Publishers, Homewood, IL, 1991.
26. Bhatia, V., Murphy, K. A., Claus, R. O., Tran, T. A. & Greene, J. A., Absolute strain and temperature measurements using high finesse EFPI cavities. *FEORC Fiber Optics Review Conference*, Blacksburg, VA, April 1994.
27. Fiber and Sensor Technologies Inc., Blacksburg, VA, AEFPI sensor technical data sheets.
28. Nawy, E. G., *Prestressed Concrete*. Prentice Hall, New Jersey, 1989.
29. de Vries, M., Bhatia, V., Claus, R. O., Murphy, K. A., Arya, V. & Tran, T., Application of absolute EFPI fiber optic sensing systems for measurement of strain in pre-tensioned tendons for pre-strained concrete. SPIE *Smart Systems for Bridges, Structures and Highways*, San Diego, CA, 26 February–3 March 1995.